A leap forward in green photochemistry: singlet fission in water solution

Chloe Magne, Simona Streckaite, Eduardo Domínguez-Ojeda, Andrea Echeverri, Flavio Siro Brigiano, Minh-Huong Ha-Thi, Marius Fanckevičius, Vidmantas Jašinskas, Annamaria Quaranta, Andrew Pascal, et al.

A leap forward in green photochemistry: singlet fission in water solution

Manuel Llansola-Portoles (manuel.llansola@i2bc.paris-saclay.fr)
Université Paris-Saclay, CEA, CNRS, Institute for Integrative Biology of the Cell (I2BC)
https://orcid.org/0000-0002-8065-9459

Chloe Magne
Université Paris-Saclay, CEA, CNRS, Institute for Integrative Biology of the Cell (I2BC)

Simona Streckaite
Center for Physical Sciences and Technology

Eduardo Domínguez-Ojeda
Insituto de Química, Universidad Nacional Autónoma de México

Andrea Echeverri
Sorbonne Université, CNRS, Laboratoire de Chimie Théorique

Flavio Siro Brigiano
Sorbonne Université, CNRS, Laboratoire de Chimie Théorique

Minh-Huong Ha-Thi
Universite Paris Saclay https://orcid.org/0000-0003-3276-1843

Marius Franckevicius
Center for Physical Sciences and Technology

Vidmantas Jasinskas
Center for Physical Sciences and Technology

Annamaria Quaranta
CEA, iBiTec-S

Andrew Pascal
Université Paris-Saclay, CEA, CNRS, Institute for Integrative Biology of the Cell (I2BC)

THOMAS Pino
CNRS https://orcid.org/0000-0002-1646-7866

Bruno Robert
Institute for Integrative Biology of the Cell (I2BC), CEA, CNRS, Université Paris-Saclay
https://orcid.org/0000-0001-5999-4538

Julia Contreras-García
Sorbonne Université, CNRS, Laboratoire de Chimie Théorique

Daniel Finkelstein-Shapiro
Insituto de Química, Universidad Nacional Autónoma de México

Vidmantas Gulbinas

Department of Molecular Compound Physics, Center for Physical Sciences and Technology

Article

Keywords: singlet fission, triplet states, triplet excitons, aqueous solution

Posted Date: October 6th, 2023

DOI: https://doi.org/10.21203/rs.3.rs-3414227/v1

Abstract

We provide the first direct evidence of singlet fission occurring with water-soluble compounds. Perylene-3,4,9,10-tetracarboxylic forms dynamic oligomers in aqueous solution, with lifetimes long enough to allow intermolecular processes such as singlet fission. As these are *transient* oligomers rather than large, stable aggregates, they retain a significant degree of disorder. We performed a comprehensive analysis of such dynamic assemblies using time-resolved absorption and fluorescence spectroscopy, nuclear magnetic resonance spectroscopy, and theoretical modelling, allowing us to observe the characteristic signatures of singlet fission and develop a model to explain the different species observed. Our findings reveal that the twist and tilt angles between perylenes are key in favoring either singlet fission or charge separation. The efficiency of triplet formation is higher than 100% and the disordered system leads to triplets living in the nanosecond time range.

Introduction

The swift development and implantation of green chemistry is essential in the current environmental emergency[1]. One battlefront for green chemistry is to run chemical reactions driven by solar energy in aqueous media, thus harnessing an unlimited energy supply (solar photons) in a medium that is both abundant and non-hazardous (water). In this framework, the development of multi-electron generation processes to boost the efficiency of photocatalysis in water offers a hypothetical solution that is yet to be exploited. Singlet fission (SF) is a spin-allowed mechanism by which a photo-excited singlet state splits into two distinct spin-triplet excited states [2]. SF was initially described in the 1950s for crystalline anthracene [3] and tetracene [4, 5, 6], and it has experienced a surge of interests due to its potential to reach photon-to-charge efficiencies up to 200%[7]. Whereas there is a lively debate around the SF mechanism and the role of intermediate species [7, 8, 9, 10, 11, 12, 13, 14], there have been no major advances in the application of SF to improve photocatalytic efficiencies. Indeed, the current scarcity of feasibility studies for SF in aqueous solution is remarkable, with only a few reports involving aqueous suspensions of diketopyrrolopyrrole nanoparticles [15] or carotenoid aggregates [16, 17, 18]. Moreover, none of these involve molecular systems *in solution*, which would simplify their coupling with molecular photocatalysts significantly. In this work, we explore the photophysics of a water-soluble organic system, characterizing the interaction(s) between molecules and its influence on their ability to undergo singlet fission or charge separation.

Results

Steady-State Absorption and fluorescence. Perylene-3,4,9,10-tetracarboxylic acid (PTC) is water soluble up to ≅100 mM. The absorption spectra in the range 0.01–90 mM (Fig. 1a, full lines) are devoid of scattering, indicating the absence of large-scale aggregation, and no absorption shifts are observed (which would be indicative of medium/strong excitonic interactions [19, 20, 21]). The vibronic peaks (414, 457, and 466 nm) display a strong concentration dependence in terms of the ratio of intensities between

the first and second vibronic peaks ($R_{abs} = \raisebox{1ex}{I_{A1}}\!\left/\!\raisebox{-1ex}{I_{A2}}\right.$), and the specific molar absorptivity (ε) (Fig. 1b). The decrease in R_{abs} is indicative of H-aggregates, whereas the lack of a blue shift, and the widening of the bands (ca. 170 cm^{-1} << ω_{vib} = 1400 cm^{-1}) support the weak nature of the excitonic couplings involved[19, 20, 21]. The hypochromism exhibited by H-aggregates has been associated with the formation of π-π-stacked species[20, 21, 22], and rationalized as the distortion, by the electronic excitation of one molecule, of the electronic states of neighboring chromophores[23]. The fluorescence spectra (Fig. 1a, dotted lines), with vibronic peaks at 481, 509, and 550 nm, exhibit strong fluorescence quenching at higher concentrations along with an increase in the ratio I^{0-0}/I^{0-1} of the vibronic emission bands, both of which are also consistent with the formation of H-aggregates[19].

^{1}H-NMR. NMR was used to characterize the interaction between PTC molecules and their resulting structure. The spectra exhibit two distinct resonances (δ1, δ2) corresponding to dissimilar protons, with a coupling constant of J = 7.9 Hz. Increasing the concentration of PTC causes an upfield shift of both resonances, starting around 40 mM (Fig. 1 c, d). The observation of a unique chemical shift for each distinct proton suggests a fast exchange between two or more chemical environments. Perylene dyes have been observed forming indefinite self-assemblies, where oligomers of different lengths coexist in dynamic equilibrium[24]. We apply an oligomer model[25] to fit the observed concentration dependence of the chemical shift (Fig. 1d), which for oligomers up to length N in equilibrium can be described by [25]:

$$\delta_{obs} = \sum_{i=1}^{N} f_i \delta_i \quad \text{(Eq. 1)}$$

Where f_i is the fractional population of molecules in an oligomer of size i, and δ_i its corresponding chemical shift. This term f_i can be calculated from:

$$f_i = \frac{{A_0}^{i-1} K^{i-1}}{(K A_0 + 1)^i} \quad \text{(Eq. 2)}$$

Where A_0 is the PTC concentration and *K* an association constant between the n-th and (n + 1)-th oligomer, which we assume is independent of oligomer size[25]. Figure 1d (red line) shows the corresponding fit for the concentration dependence of the chemical shift, using a model with oligomer size N = 5 (see *supporting information* for other models). This fitting gives an association constant of *K* = 14.8 M^{-1}. From the fractional occupations of each oligomer f_i we can then fit the observed vibrational progression R_{abs} (Fig. 1b), and obtain the electronic coupling in oligomers. We make the simplifying assumption that the electronic coupling constant is identical for oligomers of all sizes, that is, we model R_{abs} with [19]:

$$R_{abs} = f_1 + \sum_{i=2}^{N} f_i \frac{\left(1 - 0.48 \raisebox{1ex}{g}\!\left/\!\raisebox{-1ex}{ω_0}\right.\right)^2}{\left(1 + 0.146 \raisebox{1ex}{g}\!\left/\!\raisebox{-1ex}{ω_0}\right.\right)^2} \quad \text{(Eq. 3)}$$

Where g is the interchromophore coupling strength and ω_0 the frequency of the vibronic progression, in this case 1400 cm^{-1}. The fit for R_{abs} is shown on top of the experimental data in Fig. 1b (red line) for a

coupling constant of 172 cm^{-1}, fully consistent with the observed broadening of the bands (ca. 170 cm^{-1}).

Modeling. The ^{1}H-NMR measurements cannot provide any information on the molecular organization, namely: distance, tilt and twist angle between two molecules. We have run *ab initio* simulations to determine plausible structures to describe the behavior observed. Given the solubility of PTC in water, the first tests were devoted to analyzing the charge upon solution. We carried out a M06/6-31g simulation with water as implicit solvent and checked agreement of the experimental and simulated absorption spectra, obtaining a charge of (-2) on opposite sides of the molecule to present the best agreement with experimental absorption (see *Supplementary Information*). To characterize the formation of oligomers, we scanned all potential geometries and found one main dimer conformation with an intramolecular hydrogen bond (see Fig. 2a). Explicit water molecules had to be added due to the carboxylates to obtain representative results (see *Supplementary Information*). The most stable structure was re-optimized and simulated in water with *ab initio* Molecular Dynamics (ai-MD), in order to determine the variability in the twist and tilt angles (see Fig. 2a). It gave a system exhibiting large conformational variation, with an average value of (37 ± 10)º for the twist angle and a range between 0 º and 15º for the tilt angle. The evolution of the inter-layer distance reveals an average distance of 4.5 ± 0.2Å (see Fig. 2c & d).

Time Resolved fluorescence. The fluorescence decay for three PTC concentrations (10, 45 and 90 mM) has been evaluated by *single photon counting* (SPC) with ca. 200 ps resolution, giving the following decay times: 10 mM (< 200 ps & 4.0 ns), 45 mM (< 200 ps, 740 ps & 1.6 ns), 90 mM (< 200 ps). The fluorescence at higher resolution was measured by streak camera, and fitted by fixing the long components obtained by SPC. The *fluorescence decay associated species* (FDAS) yields the following components for each of the samples: 10 mM (200 & 4.0 ns), 45 mM (60, 740 & 1600 ps), and 90 mM (20 & 135 ps). This indicates the presence of π-π-stacked species even at low concentrations, which is consistent with the observations by steady state absorption and ^{1}H-NMR and probably results from hydrophobic interactions of the PTC core. The absence of any shift in the maxima or in band ratios I^{0-0}/I^{0-1} (1.1 ± 0.1) is again consistent with the presence of at least two weak H-aggregates species. It is reasonable to assume that the species decaying in 4.0 ns is monomeric PTC, while the species with shorter lifetimes correspond with singlet excimers (^{1}Ex) with different association geometries as observed in Fig. 2.

Transient absorption spectroscopy in the fs-to-ns window. The evolution of excited states after photoexcitation at 415 nm in Fig. 4 shows: dataset, gated *spectra*, and selected kinetics for 10, 45 and 90 mM PTC solutions. The 10 mM sample exhibits a distinct peak at 740 nm, which can be attributed to excited-state absorption (ESA) resulting from the $S_1 – S_n$ transition. Additionally, a negative feature at 515 nm is observed, indicating *stimulated emission* (SE). From 1 to 10 ps, there is negligible change in the spectral features. Subsequently, both the positive and negative features maintain their shape and gradually diminish in intensity at 100 and 1000 ps. This dataset can be fitted to an exponential sequential model with 3 components, attributed to singlet excimer (^{1}Ex; 200 ps), singlet monomer (S_1; 4.0

ns), and vibrationally-hot monomer/excimer ([hot-S_1/^{1}Ex]; 1 ps) (see *supplementary information*). The spectral signatures of the S_1–S_n and $^1Ex_1$–^1Ex_n transitions create an isobestic point at 585 nm. The 45 mM sample exhibits the 740 nm ESA attributed to S_1–S_n and/or $^1Ex_1$–^1Ex_n transitions, decaying at very early times (< 1 ps), and the formation of a new species with ESA at 580–610 nm which was not observed for 10 mM PTC. As observed at the isobestic point (585 nm), there is a first formation associated to short times (< 1ps), and a second ESA increase at longer times (100–1000 ps). The 90 mM sample at time zero exhibits the 740 nm ESA attributed to S_1–S_n and/or $^1Ex_1$–^1Ex_n transitions, which in this case has a lifetime less than 500 ps. Associated to the S_1–S_n and/or $^1Ex_1$–^1Ex_n transitions, a wide 580–610 nm ESA appears with higher intensity than for 45mM, suggesting that the same process occurs with higher efficiency. The sequential or parallel model fitting for 45 & 90 mM can give an approximation to the overall evolution of the system, but it is not able to produce an accurate physical description (see *supporting information*).

To produce a sound model, it is necessary to first identify the unknown species with ESA at 580–610 nm, which unfortunately is subject to controversy. For highly-coupled perylene dimers, an ESA in the 614 – 625 nm region has been assigned to singlet excimers (^{1}Ex)[26, 27]. However, it is unlikely in our weakly coupled system since we have already identified unambiguously the presence of weak coupled PTC in our diluted solutions associated to the 740 nm ESA, and we do not observe any associated fluorescence. Papadopoulos *et.al.* attributed this feature to an entangled triplet ^{1}(TT) [28], but a lifetime in the nanosecond range rules out the presence of coherent species. A 580–610 nm ESA could be due to perylene cations, but it should have the paired anion signature circa 700–750 nm [28]. The lack of any ESA for long-living species at 740 nm rules out CT in the ns time. However, polar solvents have been reported to favor CT[29], and the perylene anion signature could be obscured due to the overlap with the 740 nm ^{1}Ex-ESA. *A priori*, the triplet species of PDI derivative dimers[28, 30] and crystals [31] are reported to appear in the 600 nm region, and would be good candidates for an initial tentative assignment.

Transient absorption spectroscopy in the ns-to-µs window. Figure 5(a,b) show the dataset and decay associated spectra for ns-to-µs TA for the 90 mM sample. The dataset is fitted to a mono-exponential decay model, obtaining a component (1.3 µs) with GSB < 500 nm and ESA circa 610 nm. The lack of an ESA peak around 700–750 nm rules out the presence of perylene anions[28] and reinforces the assignment to triplet. We designed a sensitization measurement using 1H-Phenalen-1-one as sensitizer [32], which has ultrafast *inter-system crossing* (QY_{ISC} ~ 100%), to make an unequivocal assignment. The sensitization of diluted (0.1 mM) PTC in water yields a transient signature similar to the monomeric triplet reported for perylenes[28], with the main absorption ca. 550 nm and a small shoulder circa 600 nm (*see supporting information*). The most concentrated solution (90 mM) was not used since the addition of 1H-Phenalen-1-one results in reaching the solubility limit and precipitate (*see supporting information*). We therefore performed the sensitization at 45 mM, 1:1 ratio sensitizer/PTC and in 70/30 (v/v) water/ethanol to maintain solubility. Figure 5(c, d) shows the gated spectra and decay associated spectra (DAS), yielding two components (24 and 100 µs). The 100 µs DAS is coincident with the monomeric triplet observed for

dilute solution, whereas the 24 µs DAS is similar to the feature observed in the ultra-fast measurements. Hence, the only reasonable assignment for this species is triplet excimers (^{3}Ex) formed in an ultrafast manner. These triplets are only formed at high concentrations, suggesting singlet fission as their formation mechanism.

Discussion

The ^{1}H-NMR and absorption measurements suggest that there are several weak, H-type organizations of PTC in dynamic equilibrium. Theoretical modelling confirms the conformational flexibility with a distribution of distances and twist & tilt angles. The excitation energy evolution of this disordered system can be reasonably well described by a target model, featuring the parallel evolution of only two species pools (sp1 & sp2 in Fig. 6a). The deactivation rates of the singlets for each species pool is obtained from the streak camera (135 ± 5ps & 20 ± 5ps). To determine the formation rates of the new excited states for each sp, we take advantage of the isobestic point at 585 nm where only the new species absorb. Figure 6b shows the kinetics at 585 nm, that can be fitted with three formation components (1, 28 & 148 ps). The 1 ps component suggests that a small proportion of the 600 nm ESA feature is formed from Hot-S_1. The target model was fitted globally, giving 39% of sp1 and 61% of sp2. For clarity, the *Species Associated Spectra* (SAS) are shown separately for sp1 and sp2 (Fig. 6c, d, respectively). After photoexcitation, a hot-S_1 is formed to evolve in 1 ps into ^{1}Ex(sp1) and ^{1}Ex(sp2). Surprisingly, the target analysis reveals notable differences between species, not observable by sequential or parallel models. For sp1, ^{1}Ex(sp1) (green traces) generates by singlet fission (k_{sf} = (148 ps)$^{-1}$) an excited state with ESA ca. 605 nm, which was already identified as a triplet excimer (blue traces). The ^{1}Ex(sp1) SAS overlaps the Hot-S_1(sp1) SAS, apart from a small ESA in the 605 nm region. This would suggest that some of the triplet excimer is already formed from the Hot-S_1(sp1). For sp2, we observe remarkable differences for the 2nd and 3rd SAS (orange, red traces, respectively) as compared to sp1. The ^{1}Ex(sp2) SAS (orange traces) generates an excited state living 900 ps with no SE at 515 nm, and two ESA features at ca. 590 & 736 nm. The lack of fluorescence feature at 515 nm, and the long-living lifetime where no signal of fluorescence was recorded, suggest that the 736 nm ESA is not due to the $^1Ex_1 - {}^1Ex_n$ transition. These spectral features would be consistent with the formation of perylene cations and anions, respectively[28, 29]. It is worth noting that ^{1}Ex(sp2) shows a small ESA at 590 nm, which by comparison with sp1 probably forms from Hot-S_1(sp2).

The presence of different geometries leading to two different processes (CT and SF) has been described for dimers of perylene[33] and PDI[34] in organic solvents. In molecular aggregates, overlapping wavefunctions on neighboring molecules can lead to an additional CT-mediated exciton coupling with a vastly different spatial dependence and twist angle between two unslipped molecules. It has been shown that changes smaller than our modelled changes in distance and twist & tilt angles lead to a switch between CT and SF [29, 33]. However, further studies are necessary to assign each process to an exact conformation.

To calculate the efficiency of the processes (triplet and charge transfer quantum yields; Φ_T, Φ_{CT}), we cannot rely on the change in ground state bleaching due to the overlapping with the excimer triplet ESA. The most reliable method to calculate the yields of triplets and charge separation is by using the formation rates described in equations 4, 5, and 6:

$$\frac{d\left[^1Ex\right]}{dt} = -(k_r + k_{ic} + k_{isc} + k_{sf} + k_{CT})\left[^1Ex\right] \text{ (Eq. 4)}$$

$$\frac{d\left[^3Ex\right]}{dt} = (2 * k_{sf} + k_{isc})\left[^1Ex\right] \text{ (Eq. 5)}$$

$$\frac{d[CT]}{dt} = k_{CT}\left[^1Ex\right] \text{ (Eq. 6)}$$

The rate constants are denoted as follows: radiative deactivation (κ_r), internal conversion (κ_{ic}), inter-system crossing (κ_{isc}), singlet fission (κ_{sf}), and charge separation (κ_{CT}). The triplet and charge separation quantum yield are given by Eqs. 7 & 8. We consider that κ_{isc} can be approximated to zero, since no triplet formation is detected in dilute solutions. The overall singlet deactivation process is described by the singlet decay rate, measured by fluorescence and called effective singlet decay (κ_{eff}).

$$\Phi_T = \frac{d\left[^3Ex\right]}{d\left[^1Ex\right]} = \frac{2*k_{sf}+k_{isc}}{k_r+k_{nr}+k_{isc}+k_{sf}+k_{CT}} = \frac{2*k_{sf}}{k_{eff}} \text{ (Eq. 7)}$$

$$\Phi_{CS} = \frac{d[CT]}{d\left[^1Ex\right]} = \frac{k_{CT}}{k_r+k_{nr}+k_{isc}+k_{sf}+k_{CT}} = \frac{k_{CT}}{k_{eff}} \text{ (Eq. 8)}$$

Table 1
Kinetic constants for 90 mM sample obtained from the isobestic point at 585 nm, effective singlet decay (κ_{eff}) obtained by the streak camera, and quantum yield for triplet formation and charge transfer.

	%	κ_{CT} (ps^{-1})	κ_{sf} (ps^{-1})	κ_{eff} (ps^{-1})	QY triplet (%)	QY CT (%)
Specie 1	39	$(28 \pm 5)^{-1}$	N/A	$(20 \pm 5)^{-1}$	N/A	71 ± 15
Specie 2	61	N/A	$(148 \pm 10)^{-1}$	$(135 \pm 5)^{-1}$	182 ± 25	N/A

CONCLUSIONS

Our research has provided pioneering evidence of singlet fission in aqueous solutions of perylene, and yields new insights into the photophysical properties of the system. Our results show that small changes in the twisting angle can lead to different photophysical processes after photoexcitation. We calculate that the efficiency of singlet fission / charge separation in aqueous perylene oligomers depends strongly on their conformation, producing for sp1 an SF quantum efficiency close to 91% (triplet formation 182%), and for sp2 a charge separation efficiency of 70%. Overall, our study represents a major advance in the

field of singlet fission, and opens up exciting new directions for the development of more efficient solar energy technologies.

METHODS

Preparation of rylene solutions

Perylene-3,4,9,10-tetracarboxylic dianhydride (PTCDA), and Potassium Hydroxide (KOH), were purchased from Sigma-Aldrich and used as received, with a purity of 97 and 90%, respectively. To prepare perylene solutions, PTCDA was added to 0.5 M KOH in water at room temperature under continuous stirring. This results in hydrolysis of the terminal rings, yielding perylene-3,4,9,10-tetracarboxylic acid (PTC) in solution.

UV-Vis Absorption spectra were measured on a Varian Cary E5 Double-beam scanning spectrophotometer (Agilent). Hellma quartz cuvettes of varying pathlengths (10, 4, 2, 1, 0.1 and 0.01 mm) were used to accommodate the large range of PTC concentrations (over 5 orders of magnitude).

^{1}H-NMR. Stock solutions of PTC (90 mM) were prepared in 0.5 M KOH in D_2O (Sigma-Aldrich) just before use. The mixture was sonicated at room temperature for 45 min to ensure complete opening of PTCDA. All the NMR samples were prepared by diluting the corresponding volume of PTC stock solution with 0.1 M KOH, to obtain the following final concentrations: 1, 5, 10, 25, 40, 45, 50, 60, 70, 75, 80, 85 & 90 mM PTC. All samples were sonicated for 15 min just before taking the NMR spectra. ^{1}H-NMR experiments were acquired at 400 MHz with 32 scans at 25°C, in a JEOL JNM-ECZ400S spectrometer equipped with a 5 mm probe. The spectra were referenced to the solvent peak at 4.81 ppm, and the pure chemical shifts are reported along with the J coupling splitting. The fits are performed using the most downfield shifted resonance.

Nano-to-millisecond transient absorption was performed on an Edinburgh Instruments LP920 Flash Photolysis Spectrometer system, incorporating a Continuum Surelite OPO. The OPO was pumped by a Q-switched Nd:YAG laser operating at 355 nm, having a pulse duration of 5 ns. The LP920 system is equipped with a 450 W pulsed Xenon arc lamp as the probe for the transient absorption measurements. Detection in the LP920 system is performed either via a Czerny-Turner blazed 500-nm monochromator (bandwidth 1–5 nm) coupled with a Hamamatsu R928 photomultiplier tube (kinetics mode), or via a 500-nm-blazed spectrograph (bandwidth 5 nm) coupled with a water-cooled ICCD nanosecond Andor DH720 camera (spectral mode). The samples had absorbance of ~ 0.8 at the excitation wavelength and the energy of the laser pulse was ~ 10 mJ.

Femto–to–nanosecond time-resolved transient absorption. The ultrafast transient absorption (TA) setup was based on an amplified femtosecond laser Pharos 10-600-PP (Light Conversion Ltd., Lithuania), operating at a fundamental wavelength of 1030 nm, with a repetition rate of 50 kHz and a pulse width of ~ 230 fs. A collinear optical parametric amplifier Orpheus PO15F2L (Light Conversion Ltd., Lithuania) was used to obtain 415 nm wavelength pulses for sample excitation. The measurements were performed

at a repetition rate of 4.554 kHz frequency, achieved by using the pulse picker. Excitation was modulated by mechanical chopper synchronized to the output of the pulse picker. As a probe, we used laser pulses, spectrally broadened by means of continuum generation in a sapphire crystal. The time delay between the pump and probe pulses was varied by an optical delay line based on retroreflector optics mounted on an Aerotech PRO165LM electromechanical translation stage (Aerotech Ltd., UK). The detection equipment consisted of an Andor-Shamrock SR-500i-B1-R spectrometer (Andor Technology, UK) with 150 lines/mm diffraction grating equipped with Andor-Newton DU970 CCD camera (1600 × 200 pixels; Andor Technology Ltd., UK). The reading of the camera was synchronized with the chopper. The data was recorded and processed using home-written software in the LabView programming environment. The changes in absorption (ΔA) were measured as a function of both the wavelength and time delay between pump and probe pulses.

Picosecond time-resolved fluorescence was performed with a streak camera system (Hamamatsu C5680) with synchroscan (M5675) unit coupled to a spectrometer. A femtosecond Yb:KGW oscillator (Light Conversion Ltd., Lithuania) generating 80 fs duration pulses at 1030 nm, which were frequency tripled to 343 nm (HIRO harmonics generator, Light Conversion Ltd.) at a repetition rate of 76 MHz, was used for the sample excitation. Excitation energy density was attenuated using neutral density filters to about 15 nJ·cm − 2. The time resolution of the system was ≈ 8 ps. Signal acquisition time was 1–3 h for each measurement.

Pico-to-nanosecond time-resolved fluorescence was performed with an Edinburgh F920 spectrometer (Edinburgh Instruments, UK). Fluorescence decay kinetics were obtained using time-correlated single photon counting (TCSPC). The excitation source was a picosecond-pulsed diode laser EPL-375 (Edinburgh Instruments, UK) emitting ∼60 ps pulses (5 MHz repetition rate). Temporal resolution of this system was a few hundred ps.

Simulations. Optimized molecular structures, vibrational frequencies and excited states were calculated using Gaussian 16 software. All calculations have been performed with an implicit solvent model (PCM), where a dielectric constant of 78.35 was used to simulate the aqueous solvent. The configurational search for dimers was performed by placing the monomers in the center of cubes of various sizes and allowed to evolve under annealing conditions according to the inner workings of the ASCEC program. Following the generation of candidate structures to be minima on the potential energy surface, these structures were subsequently optimised and classified as true minima by evaluation of the eigenvalues of the Hessian matrix at the DFT level of theory, using the M06 functional and the 3-21G basis set.

The most stable dimer structure was then simulated by ai-MD in presence of bulk water by means of CP2K/Quickstep code[35], which is optimally designed for massive parallel computing. The liquid phase was modeled with 432 water molecules in a cubic box with an edge length of 24.312 Å ($\rho_{H2O} \approx 1.0$ g cm^3), generated by PACKMOL software[36, 37]. The final model was generated by adding to the simulation box the perylene dimer structure previously optimized by quantum static calculations in the presence of few explicit molecules in PCM. The dimensions of the box lead to a minimal distance between the replica

of 12.5 Å along the dynamics. The neutrality of the box was ensured by adding four K^+ ions into the simulation boxes, in positions close to the perylene carboxylate groups. Throughout the entire 30 ps duration of the molecular dynamics simulation, the K^+ ions remained situated within the first solvation shell of the perylenes. The system was equilibrated for 13 ps and only the last 17 ps of simulation has been analyzed. Before running the ai-MD simulation, the positions of all the atoms in the simulation boxes were optimized at T = 0 K, adopting the same set-up and electronic description of the dynamics. We adopted Born–Oppenheimer molecular dynamics (BOMD), the PBE[37] approximation of density functional theory together with Grimme's D3(BJ) correction for the description of dispersion interactions[38, 39], GTH pseudopotentials[40, 41], combined plane-wave (600 Ry cutoff) and DZVP-MOLOPT-SR basis sets. The ai-MD simulations were carried out in the spin-restricted Kohn–Sham scheme. We adopted the Nosé–Hoover thermostat[42, 43] to control the average temperature at 300 K in the NVT ensemble. The length of the Nosé–Hoover chain was equal to 3, whereas the time constant of the thermostat was set to 100 fs, with the third-order Yoshida integrator and multiple time step set to 2. Trajectories of 1 ps, with a time step of 0.5 fs, were found to be sufficiently long to reach the target temperature. The MD simulations were run for a total of 20 ps, and only the last 15 ps were considered for analysis. VMD[44] software was used to visualize the MD trajectories and the analysis on the dimer twist angle fluctuations was performed with the Travis package[45, 46].

Declarations

Acknowledgements

This work was supported by the French Infrastructure for Integrated Structural Biology (FRISBI) ANR-10-INBS-05, the French National Research Agency (SINGLETFISSION grant N°: ANR-23-CE29-0007 and FISCIENCY grant N°: ANR-23-CE50), the CNRS 80PRIME interdisciplinary program, and ECOS-Nord program (action #M21P02). DFS acknowledges funding from PAPIIT IA202821. We acknowledge Elisabet Huerta for technical assistance. The authors thank the Grand Equipement National de Calcul Intensif (GENCI) French National Supercomputing Facility for computer time (project Grant A0140814154).

References

1. Anastas P, Eghbali N. Green Chemistry: Principles and Practice. Chem Soc Rev 2010, 39(1): 301–312.
2. Smith MB, Michl J. Singlet Fission. Chem Rev (Washington, DC, U S) 2010, 110(11): 6891–6936.
3. Singh S, Jones WJ, Siebrand W, Stoicheff BP, Schneider WG. Laser Generation of Excitons and Fluorescence in Anthracene Crystals. J Chem Phys 1965, 42(1): 330–342.
4. Swenberg CE, Stacy WT. Bimolecular radiationless transitions in crystalline tetracene. Chem Phys Lett 1968, 2(5): 327–328.

5. Geacintov N, Pope M, Vogel F. Effect of Magnetic Field on the Fluorescence of Tetracene Crystals: Exciton Fission. Phys Rev Lett 1969, 22(12): 593–596.
6. Merrifield RE, Avakian P, Groff RP. Fission of singlet excitons into pairs of triplet excitons in tetracene crystals. Chem Phys Lett 1969, 3(3): 155–157.
7. Casillas R, Papadopoulos I, Ullrich T, Thiel D, Kunzmann A, Guldi DM. Molecular insights and concepts to engineer singlet fission energy conversion devices. Energy & Environmental Science 2020, 13: 2741–2804
8. Pandya R, Gu Q, Cheminal A, Chen RYS, Booker EP, Soucek R, *et al.* Optical Projection and Spatial Separation of Spin-Entangled Triplet Pairs from the S1 (21 Ag–) State of Pi-Conjugated Systems. Chem 2020, 6(10): 2826–2851.
9. Musser AJ, Clark J. Triplet-Pair States in Organic Semiconductors. Annu Rev Phys Chem 2019, 70(1): 323–351.
10. Walker BJ, Musser AJ, Beljonne D, Friend RH. Singlet exciton fission in solution. Nature Chem 2013, 5(12): 1019–1024.
11. Stern HL, Musser AJ, Gelinas S, Parkinson P, Herz LM, Bruzek MJ, *et al.* Identification of a triplet pair intermediate in singlet exciton fission in solution. Proc Natl Acad Sci 2015, 112(25): 7656–7661.
12. Dover CB, Gallaher JK, Frazer L, Tapping PC, Petty AJ, Crossley MJ, *et al.* Endothermic singlet fission is hindered by excimer formation. Nature Chem 2018, 10(3): 305–310.
13. Bossanyi DG, Matthiesen M, Wang S, Smith JA, Kilbride RC, Shipp JD, *et al.* Emissive spin-0 triplet-pairs are a direct product of triplet–triplet annihilation in pentacene single crystals and anthradithiophene films. Nature Chem 2021, 13(2): 163–171.
14. Tayebjee MJY, Sanders SN, Kumarasamy E, Campos LM, Sfeir MY, McCamey DR. Quintet multiexciton dynamics in singlet fission. Nat Phys 2017, 13(2): 182–188.
15. Grzybowski M, Gryko DT. Diketopyrrolopyrroles: Synthesis, Reactivity, and Optical Properties. Advanced Optical Materials 2015, 3(3): 280–320.
16. Musser AJ, Maiuri M, Brida D, Cerullo G, Friend RH, Clark J. The Nature of Singlet Exciton Fission in Carotenoid Aggregates. J Am Chem Soc 2015, 137(15): 5130–5139.
17. Quaranta A, Krieger-Liszkay A, Pascal AA, Perreau F, Robert B, Vengris M, *et al.* Singlet fission in naturally-organized carotenoid molecules. Phys Chem Chem Phys 2021, 23(8): 4768–4776.
18. Llansola-Portoles MJ, Redeckas K, Streckaité S, Ilioaia C, Pascal AA, Telfer A, *et al.* Lycopene crystalloids exhibit singlet exciton fission in tomatoes. Phys Chem Chem Phys 2018, 20(13): 8640–8646.
19. Hestand NJ, Spano FC. Expanded Theory of H- and J-Molecular Aggregates: The Effects of Vibronic Coupling and Intermolecular Charge Transfer. *Chem Rev (Washington, DC, U S)* 2018, 118(15): 7069–7163.
20. Dehm V, Chen Z, Baumeister U, Prins P, Siebbeles LDA, Würthner F. Helical Growth of Semiconducting Columnar Dye Assemblies Based on Chiral Perylene Bisimides. Org Lett 2007, 9(6): 1085–1088.

21. Syamala PPN, Soberats B, Görl D, Gekle S, Würthner F. Thermodynamic insights into the entropically driven self-assembly of amphiphilic dyes in water. Chemical Science 2019, 10(40): 9358–9366.
22. Spano FC. The Spectral Signatures of Frenkel Polarons in H- and J-Aggregates. Acc Chem Res 2010, 43(3): 429–439.
23. Cantor CR, Schimmel P. 7 Absorption Spectroscopy. *Biophysical Chemistry: Part II: Techniques for the Study of Biological Structure and Function*, 1980.
24. Shaller AD, Wang W, Gan H, Li ADQ. Tunable Molecular Assembly Codes Direct Reaction Pathways. Angew Chem Int Ed 2008, 47(40): 7705–7709.
25. Wang W, Han JJ, Wang L-Q, Li L-S, Shaw WJ, Li ADQ. Dynamic π – π Stacked Molecular Assemblies Emit from Green to Red Colors. Nano Lett 2003, 3(4): 455–458.
26. Cook RE, Phelan BT, Kamire RJ, Majewski MB, Young RM, Wasielewski MR. Excimer Formation and Symmetry-Breaking Charge Transfer in Cofacial Perylene Dimers. J Phys Chem A 2017, 121(8): 1607–1615.
27. Ni W, Gurzadyan GG, Zhao J, Che Y, Li X, Sun L. Singlet Fission from Upper Excited Electronic States of Cofacial Perylene Dimer. J Phys Chem Lett 2019, 10(10): 2428–2433.
28. Papadopoulos I, Gutiérrez-Moreno D, Bo Y, Casillas R, Greißel PM, Clark T, *et al.* Altering singlet fission pathways in perylene-dimers; perylene-diimide versus perylene-monoimide. Nanoscale 2022, 14(13): 5194–5203.
29. Margulies EA, Miller CE, Wu Y, Ma L, Schatz GC, Young RM, *et al.* Enabling singlet fission by controlling intramolecular charge transfer in π-stacked covalent terrylenediimide dimers. Nature Chem 2016, 8(12): 1120–1125.
30. Yu Z, Wu Y, Peng Q, Sun C, Chen J, Yao J, *et al.* Accessing the Triplet State in Heavy-Atom-Free Perylene Diimides. Chemistry – A European Journal 2016, 22(14): 4717–4722.
31. Nagarajan K, Mallia AR, Reddy VS, Hariharan M. Access to Triplet Excited State in Core-Twisted Perylenediimide. J Phys Chem C 2016, 120(16): 8443–8450.
32. Flors C, Nonell S. On the Phosphorescence of 1H-Phenalen-1-one. Helv Chim Acta 2001, 84(9): 2533–2539.
33. Hestand NJ, Spano FC. Interference between Coulombic and CT-mediated couplings in molecular aggregates: H- to J-aggregate transformation in perylene-based π-stacks. J Chem Phys 2015, 143(24): 244707.
34. Idé J, Méreau R, Ducasse L, Castet F, Olivier Y, Martinelli N, *et al.* Supramolecular Organization and Charge Transport Properties of Self-Assembled π – π Stacks of Perylene Diimide Dyes. J Phys Chem B 2011, 115(18): 5593–5603.
35. VandeVondele J, Krack M, Mohamed F, Parrinello M, Chassaing T, Hutter J. Quickstep: Fast and accurate density functional calculations using a mixed Gaussian and plane waves approach. Comput Phys Commun 2005, 167(2): 103–128.

36. Martínez JM, Martínez L. Packing optimization for automated generation of complex system's initial configurations for molecular dynamics and docking. J Comput Chem 2003, 24(7): 819–825.
37. Martínez L, Andrade R, Birgin EG, Martínez JM. PACKMOL: A package for building initial configurations for molecular dynamics simulations. J Comput Chem 2009, 30(13): 2157–2164.
38. Perdew JP, Burke K, Ernzerhof M. Generalized Gradient Approximation Made Simple. Phys Rev Lett 1996, 77(18): 3865–3868.
39. Grimme S, Antony J, Ehrlich S, Krieg H. A consistent and accurate ab initio parametrization of density functional dispersion correction (DFT-D) for the 94 elements H-Pu. J Chem Phys 2010, 132(15).
40. Grimme S, Ehrlich S, Goerigk L. Effect of the damping function in dispersion corrected density functional theory. J Comput Chem 2011, 32(7): 1456–1465.
41. Goedecker S, Teter M, Hutter J. Separable dual-space Gaussian pseudopotentials. Physical Review B 1996, 54(3): 1703–1710.
42. Hartwigsen C, Goedecker S, Hutter J. Relativistic separable dual-space Gaussian pseudopotentials from H to Rn. Physical Review B 1998, 58(7): 3641–3662.
43. Nosé S. A molecular dynamics method for simulations in the canonical ensemble. Mol Phys 1984, 52(2): 255–268.
44. Humphrey W, Dalke A, Schulten K. VMD: Visual molecular dynamics. Journal of Molecular Graphics 1996, 14(1): 33–38.
45. Brehm M, Thomas M, Gehrke S, Kirchner B. TRAVIS—A free analyzer for trajectories from molecular simulation. J Chem Phys 2020, 152(16).
46. Brehm M, Kirchner B. TRAVIS - A Free Analyzer and Visualizer for Monte Carlo and Molecular Dynamics Trajectories. J Chem Inf Model 2011, 51(8): 2007–2023.

Figures

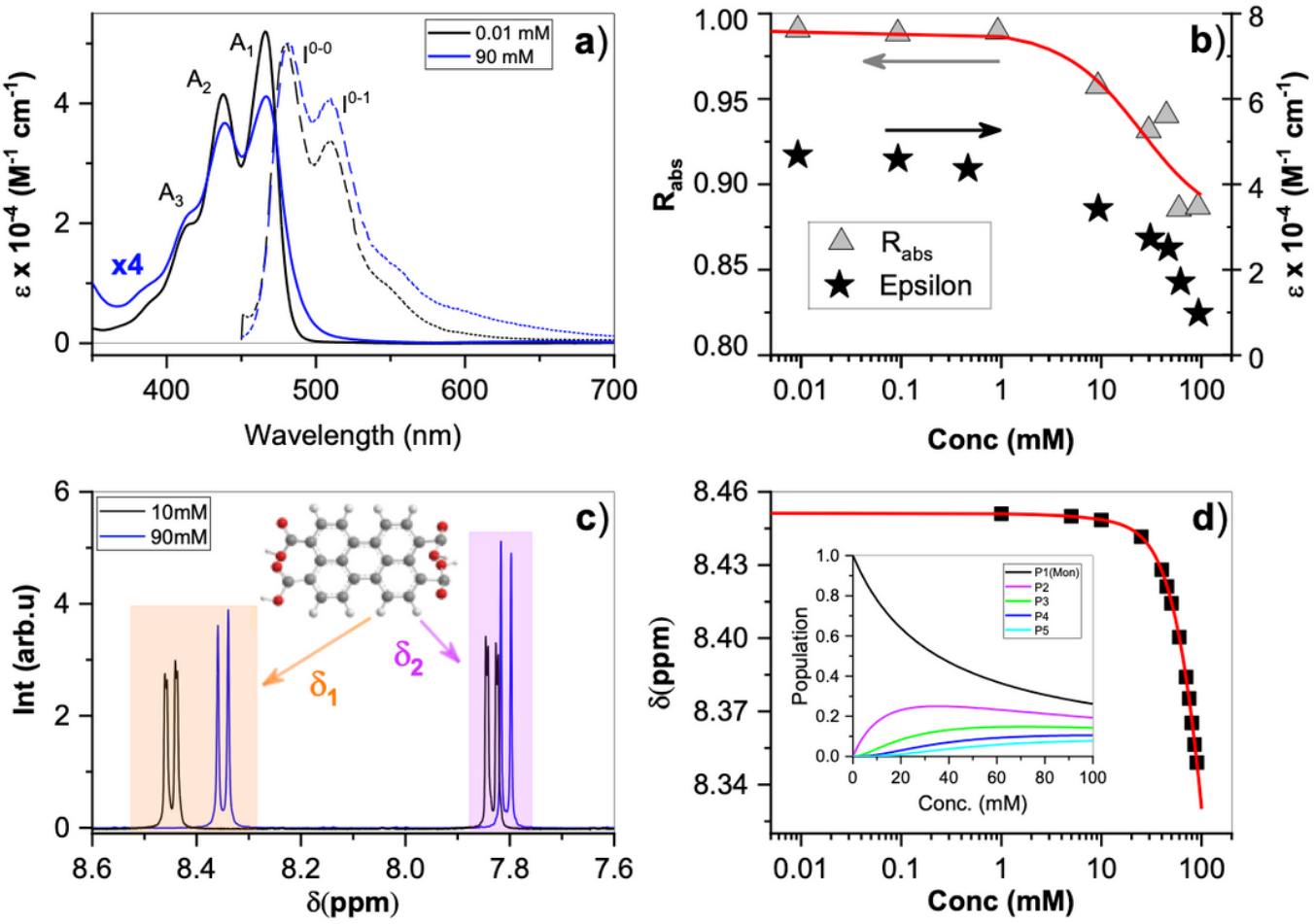

Figure 1

a) Room temperature absorption, represented as molar absorption coefficient (e), and normalized fluorescence of PTC at 0.01 and 90 mM. **b)** Variation of e at 466 nm (black stars – right y-axis) and R_{abs} (grey triangles – left y-axis) with concentration. The red line is the fitting of R_{abs} using equation 3. **c)** Chemical shifts showing two distinct environments for the protons (d_1 orange & d_2 violet) marked in the molecular structure. **d)** Chemical shift as a function of concentration (black squares) and model fitting using equation 2 (red line). **Inset**: evolution of monomer and oligomer populations with concentration.

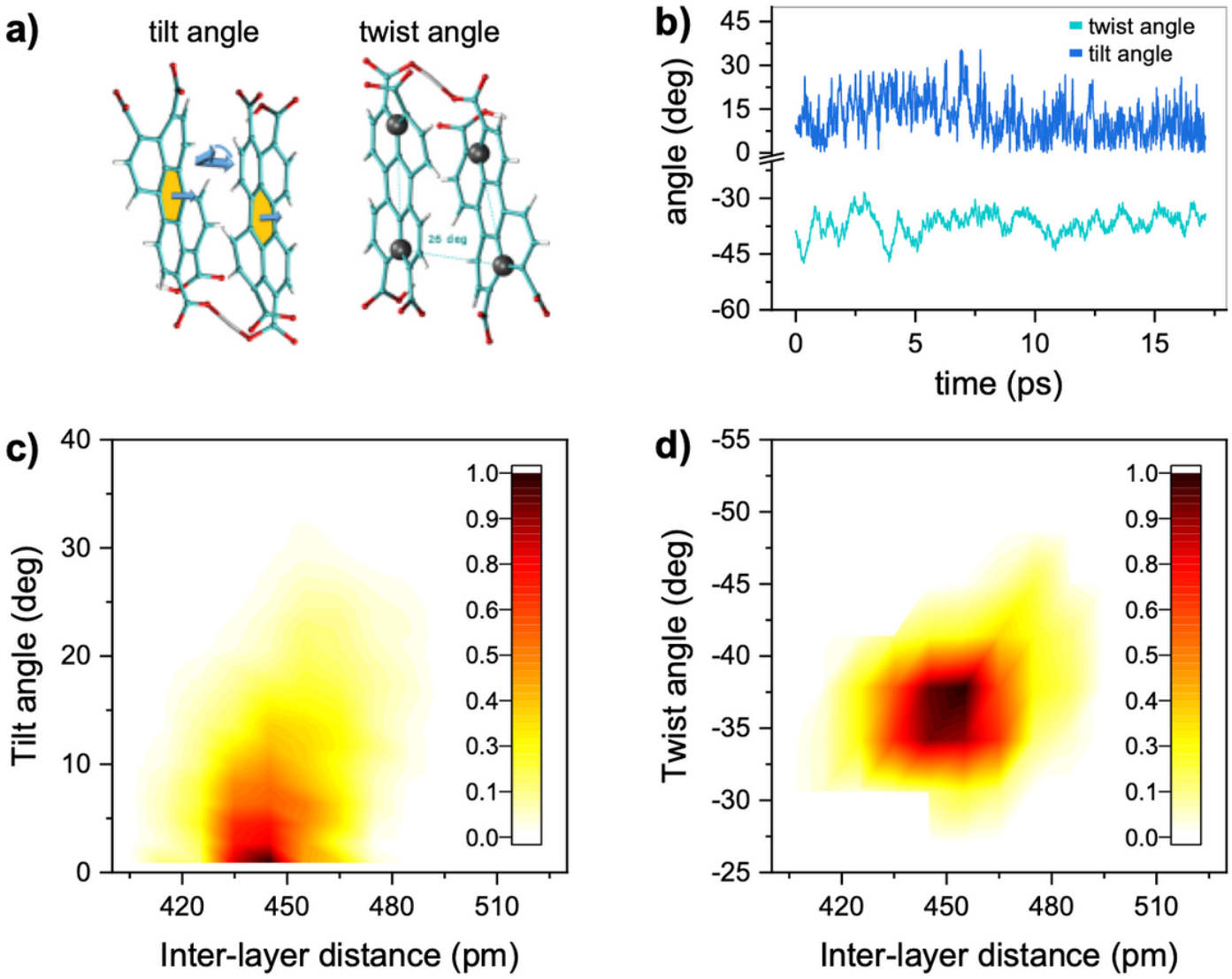

Figure 2

a) Schematic representation of the dimer twist and tilt angles considered. The tilt angle is defined as the angle between the two vectors perpendicular to the central C_6 units of each monomer. The twist angle is defined as the dihedral angle formed from the three consecutive vectors connecting the four carbon atoms which are represented as grey spheres. **b)** Temporal evolution of the twist and tilt angles (light and dark blue, respectively) along the ai-MD trajectory at 300 K. Combined angular/radial probability of **c)** the twist angle and **d)** the tilt angle with respect to the distance between the two monomers computed from the ai-MD trajectory.

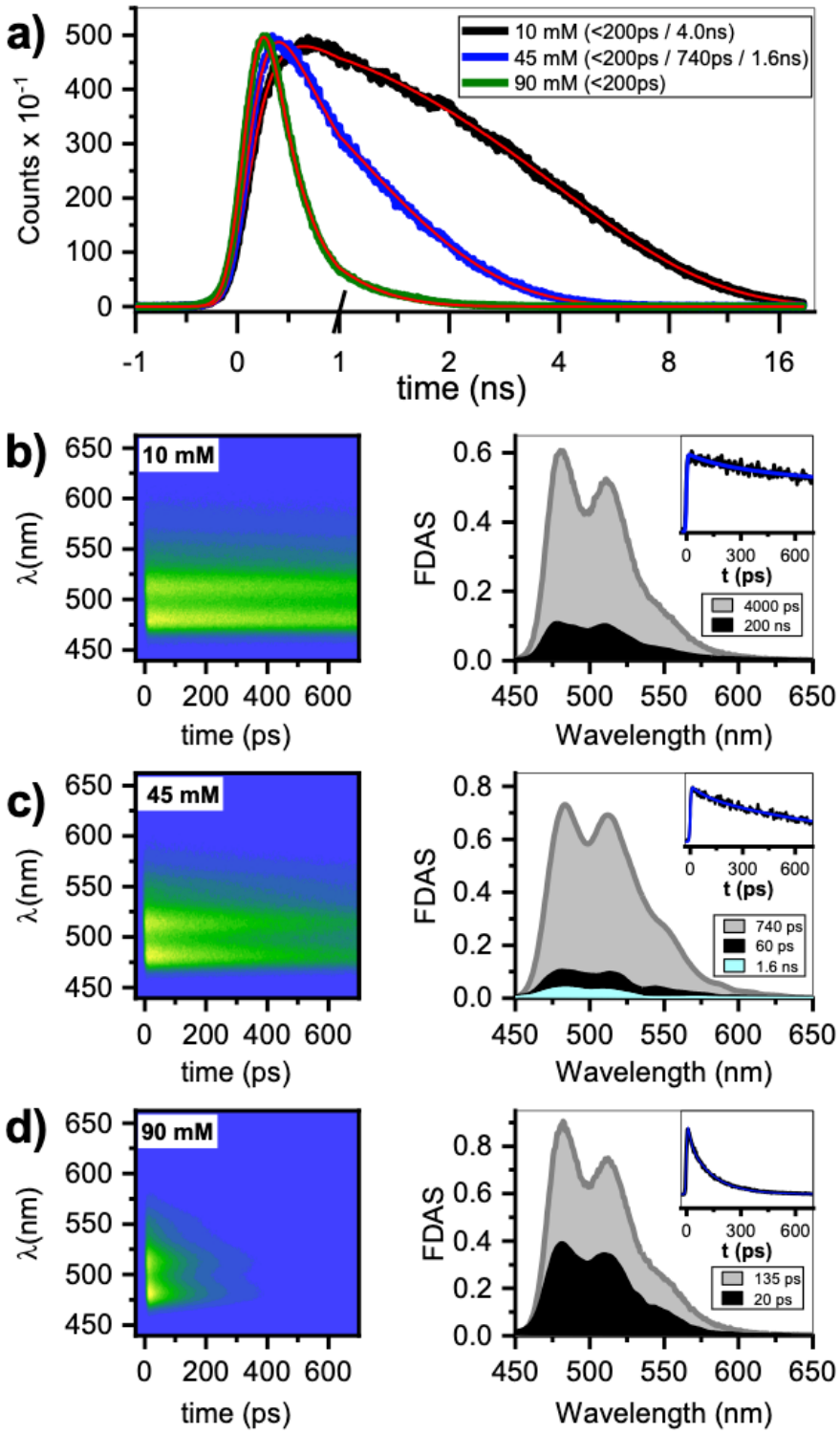

Figure 3

a) Single photon counting collected at 510 nm upon 415 nm excitation for 10, 45 & 90 mM PTC solutions. Time-spectral 2D fluorescence matrix collected by streak camera, fluorescence decay associated species (FDAS), and kinetics at 510 nm from **b)** 10 mM, **c)** 45 mM & **d)** 90 mM solution. The OD was adjusted to less than 0.1 to minimize self-absorption distortion, the excitation was at 343 nm and the excitation energy ~15 nJ·cm^2.

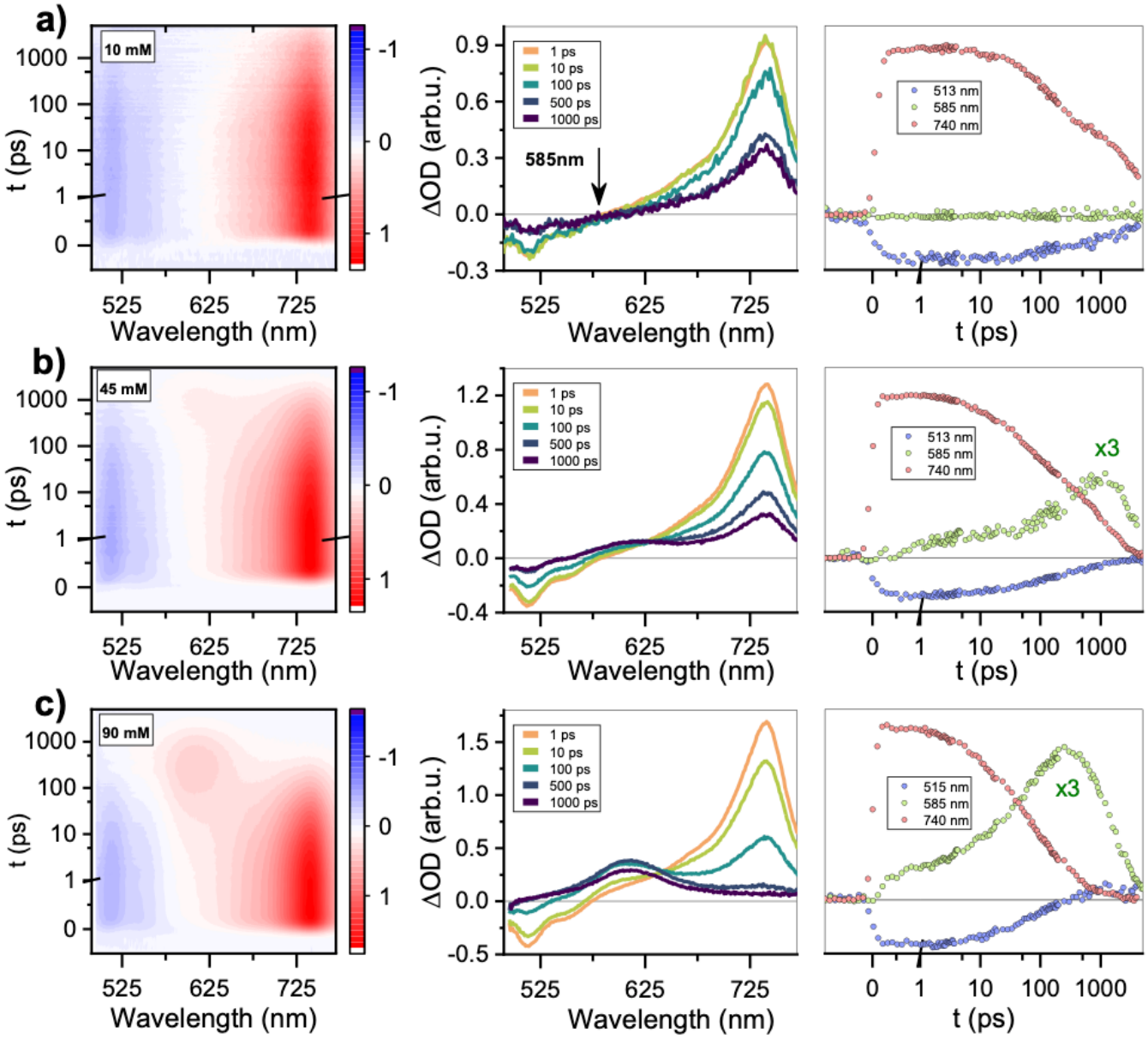

Figure 4

Transient absorption spectra of PTC in the fs-to-ns window: time-spectral map, gated-spectra at 1, 10, 100, 500, and 1000 ps, and kinetics at 515, 585, and 740 nm for **a)** 10 mM, **b)** 45 mM, **c)** 90 mM solution. Excitation wavelength at 415 nm and power 100 mW.

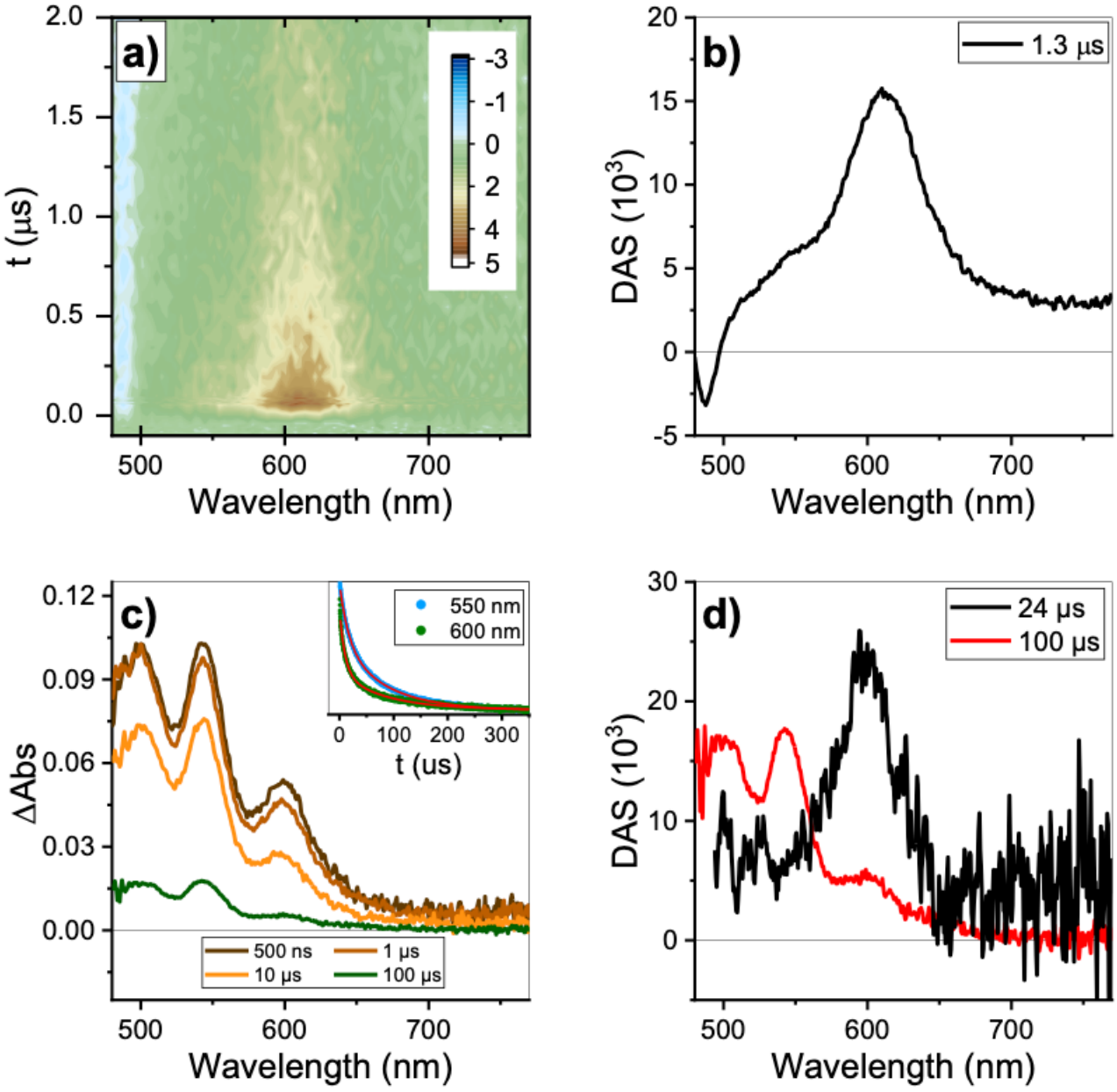

Figure 5

a) Dataset of transient absorption in the ns-to-µs window, and **b)** decay associated spectra (DAS) for 90 mM solution. **c)** Gated spectra, kinetics (*inset*) and **d)** DAS of 45 mM PTC in 70/30 (v/v) water/ethanol upon sensitization with 1H-Phenalen-1-one (excitation at 350 nm).

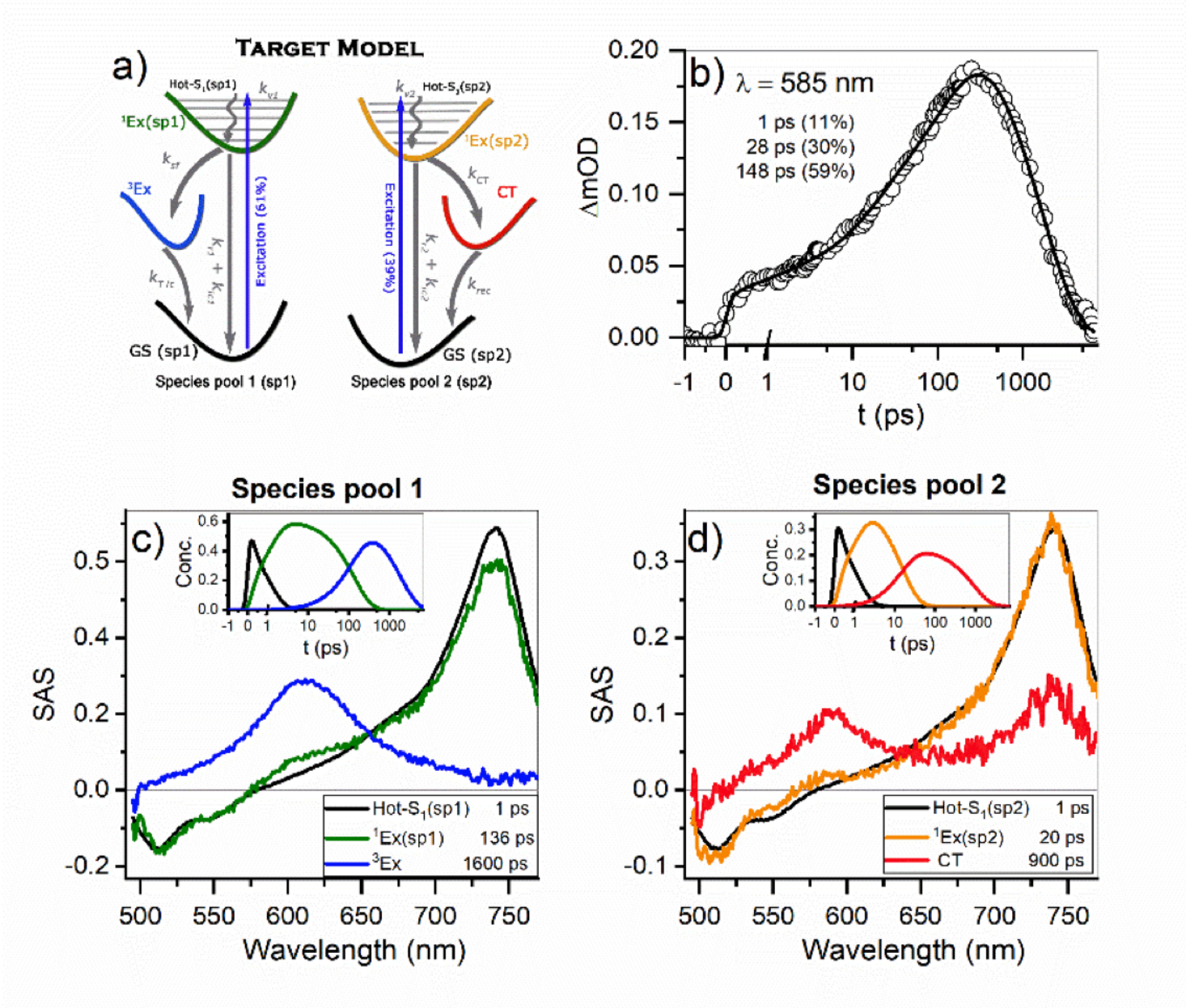

Figure 6

a) Target model for two dimers decaying in parallel. The electronic levels are color-coded with the associated SAS obtained from the global fitting. The system evolves as follows for sp1 (sp2): Hot-S_1 – grey (black), ^{1}Ex - green (orange) and unknown species - blue (red). **b)** Kinetics and fitting of the isobestic point (585 nm) for 90 mM PTC. **c,d)** SAS for 90 mM PTC with 415 nm excitation at 100 mW for sp1 & sp2.

Supplementary Files

This is a list of supplementary files associated with this preprint. Click to download.

- Supportinginformation.docx